Data-Driven Koopman Based Fractional Order PID Control of a MEMS Gyroscope Using Bat Algorithm

Mehran Rahmani and Sangram Redkar

The Polytechnic School, Ira Fulton School of Engineering, Arizona State University, Mesa, AZ 85212

Abstract: Data-driven control methods provide robust techniques for controlling the systems with a non-linear dynamic model. This paper uses the Koopman operator to linearize the non-linear dynamic model. Generating the Koopman operator is the critical part of using the Koopman theory. First, dynamic mode decomposition (DMD) is used to obtain eigenfunctions for producing the Koopman operator. Then, a fractional order PID (FOPID) controller is applied to control the linearized dynamic model. Finally, a swarm intelligence bat optimization algorithm is utilized to tune the FOPID controller's parameters. In comparison to Micro-electromechanical systems (MEMS) gyroscope controlled by a conventional PID controller, FOPID, Koopman-based FOPID controller (Koopman-FOPID), and Koopman-FOPID control optimized by bat algorithm (Koopman-BAFOPID) show better performance in comparison with three other controllers in terms of high tracking performance, low tracking error, and low control efforts.

Keywords: Bat algorithm, Fractional PID control, Koopman operator, Dynamic mode decomposition, MEMS gyroscope, Data-driven method.

1. Introduction

The 2D MEMS gyroscope can measure angular velocities in the x and y directions. This tool has been used in the automotive industry due to its low costs and small size [1, 2]. However, controlling the MEMS gyroscope is problematic because it is constantly subjected to external disturbances.

An exciting area of study is the data-driven control system, which uses a data-driven model to control the dynamical systems [3-5]. Several techniques are used to create data-driven structures, such as deep neural networks [6] and machine learning algorithms [7]. In data-driven control systems, Koopman theory is a robust approach. By projecting the system dynamics onto the Koopman eigenspace, Goswami and Paley [8] explore the issues of bilinearization and optimum control of a control-affine non-linear system. Under certain assumptions, the suggested technique

converts the dynamics into a bilinear system using the Koopman canonical transform, especially the Koopman eigenfunctions of the drift vector field. Numerous examples of control-affine non-linear systems are used to numerically demonstrate bilinearization and the best control strategy while assuming a quadratic cost function for the states and control input. However, models created using model-based control design methodologies make it challenging to operate soft robots precisely. Koopman operator theory provides a framework for creating explicit dynamical models of soft robotics and controlling them with practiced model-based techniques [9]. The most crucial aspect of the Koopman theory is how to derive the Koopman operator, especially for complex systems with non-linear dynamic systems.

A helpful approach for estimating the modes and eigenvalues of the Koopman operator is the DMD method. Utilizing an embedding into infinite dimensional space, the Koopman operator offers a linear description of the non-linear system. The most often used finite dimensional approximations of the Koopman Operator are DMD and Extended DMD [10,11]. Koopman operator theory and the associated algorithm DMD were introduced by Ling et al. for the study and control of signalized traffic flow networks. They studied DMD's application to various issues in signalized traffic as a model-free method for describing complicated oscillatory dynamics from observed data [12]. Wilches-Bernal et al. [13] proposed a novel technique for identifying faults and other power quality issues. Their study demonstrated how one might detect events using current and voltage data to discriminate between different failures. The performance of the strategy is examined concerning the impact of the window size because the suggested method is window-based. To properly control the system, an appropriate controller can be used with the linearized DMD Koopman model, such as a linear quadratic regulator controller (LQR) [14] and a model predictive controller (MPC) [15].

PID controller is a powerful control method to control linear dynamic systems. It has been widely used in real-world scenarios due to its low cost and ease of implementation [16, 17]. It is used to control different systems, such as MEMS gyroscopes [18], vehicles [19], and quadcopters [20]. However, the main drawbacks of the PID control method are that it's not robust control against external disturbances. Fractional control is a suitable controller to improve the robustness and stability of the PID controller. FOPID controller has been used in other research. Significant uncertainty in dynamic and hydrodynamic properties and the signal transmission channel's time

delay are the key challenges with autonomous underwater vehicles (AUV) motion control. For an AUV yaw control system, Liu et al. suggested a reliable FOPID controller architecture [21]. Erol [22] proposed a method using the pitch control system of large wind turbines with a FOPID delay-dependent controller. The simulation findings demonstrate that outcomes for the delay margin are improved by using the proposed method. One of the main parts of FOPID controller design is tuning the controller's gains to achieve the best performance. The bat optimization algorithm is suitable for adjusting the proposed controller's parameters.

The bat algorithm is inspired by the behavior of microbats that use echolocation, with varying pulse rates of emission and loudness [23]. Based on the Equivalent Transfer Function model and a reduced decoupler, the [24] describes a technique for developing independent FOPID controllers for two interacting conical tank level processes. In addition, an optimization bat algorithm was used to increase the power system stability by tuning FOPID controller parameters in reference [25].

This research paper proposes a new data-driven control algorithm to control the MEMS gyroscope. The contributions of this work are as follows:

1- The non-linear dynamic model of the MEMS gyroscope is presented.

2- DMD method is used to generate eigenfunction and eigenvectors to obtain Koopman operator.

3- Using the Koopman theory, a FOPID controller is implemented to control the linearized dynamic model.

4- A bat metaheuristic optimization algorithm is used to tune the proposed control method parameters.

The rest of this paper is arranged as follows. Section two discusses the dynamic model of the MEMS gyroscope. Section three presents the Koopman theory. Section four describes the DMD method. Section five explains PID and FOPID control methods. Section six discusses the bat algorithm. Section seven provides the simulation results. Finally, section eight presents the conclusion.

2- Non-linear dynamic model of MEMS gyroscope

The MEMS gyroscope is a sensor for angular velocity measurement using x and y motion [26-28]. This device has been used in the automotive industry. A typical z-axis MEMS gyroscope architecture is shown in Figure 1.

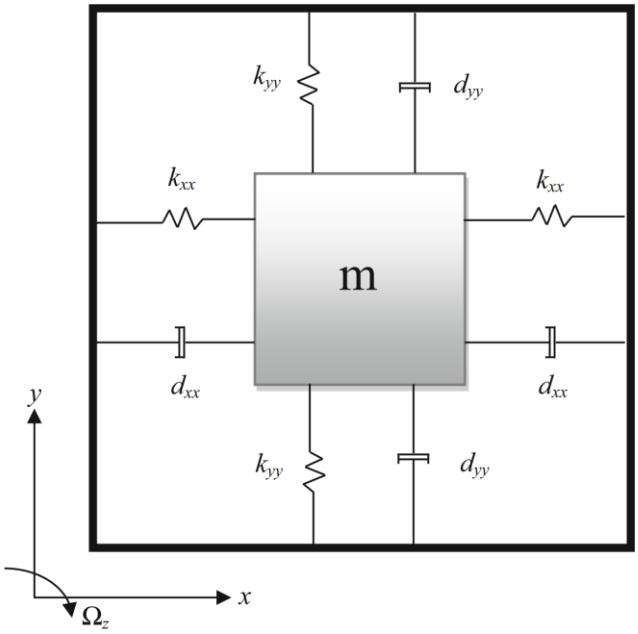

Fig. 1. MEMS gyroscope structure [21].

A typical MEMS gyroscope design includes sensor mechanisms, a proof mass suspended by springs, and an electrostatic actuation system for generating an oscillatory motion and determining the position and speed of the proof mass [29]. The proof mass is mounted on a frame that moves with a consistent linear velocity while the gyroscope rotates at a gradually varying angular velocity, Ω_z. The centrifugal forces $m\Omega_z^2 x$ and $m\Omega_z^2 y$ are expected to be insignificant due to the modest displacements x and y. The development of the Coriolis forces, $2m\Omega_z^* \dot{y}$ and $2m\Omega_z^* \dot{x}$, is parallel to the driving and rotating axes [30]. The following equations describe the dynamics of the gyroscope.

$$m\ddot{x} + d_{xx}^* \dot{x} + d_{xy}^* \dot{y} + k_{xx}^* x + k_{xy}^* y + \beta x^3 = u_x^* + 2m\Omega_z^* \dot{y} \quad (1)$$

$$m\ddot{y} + d_{xy}^* \dot{y} + d_{yy}^* \dot{y} + k_{xy}^* x + k_{yy}^* y + \beta y^3 = u_y^* - 2m\Omega_z^* \dot{x} \quad (2)$$

The origin of the coordinates in equations 1 and 2 is placed in the center of the proof mass since there is no external force applied to the system. The constants k_{xy}^* and d_{xy}^*, respectively, stand in for the asymmetric spring and damping coefficients. Despite the possibility of minor unknown deviations from their nominal values, the control forces in the x- and y-direction, u_x^* and u_y^*, are usually accepted. There are also typical descriptions of the damping rates, d_{xx}^* and d_{yy}^* and the spring constants of springs interacting in the x- and y-directions, $k_{xx}^*$and k_{yy}^*. Therefore, both electro-mechanical and mechanical nonlinearity, which is a positive constant, will introduce the terms βx^3 and βy^3. The following vector representation might be used to express equations 1 and 2:

$$\frac{\ddot{q}^*}{q_0} + \frac{D^*}{m\omega_0}\frac{\dot{q}^*}{q_0} + \frac{K_a}{m\omega_0^2}\frac{q^*}{q_0} + \beta\frac{{q^*}^3}{q_0} = \frac{u^*}{m\omega_0^2 q_0} - 2\frac{\Omega^*}{\omega_0}\frac{\dot{q}^*}{q_0} \tag{3}$$

where

$$q^* = \begin{bmatrix} x^* \\ y^* \end{bmatrix}, \quad u = \begin{bmatrix} u_x^* \\ u_y^* \end{bmatrix}, \quad \Omega^* = \begin{bmatrix} 0 & -\Omega_z^* \\ \Omega_z^* & 0 \end{bmatrix}, \quad D^* = \begin{bmatrix} d_{xx}^* & d_{xy}^* \\ d_{xy}^* & d_{yy}^* \end{bmatrix}, \quad K_a = \begin{bmatrix} k_{xx}^* & k_{xy}^* \\ k_{xy}^* & k_{yy}^* \end{bmatrix}$$

And non-dimensional parameters are as follows:

$$q = \frac{q^*}{q_0} \qquad d_{xy} = \frac{d_{xy}^*}{m\omega_0} \qquad \Omega_z = \frac{\Omega_z^*}{\omega_0} \tag{4}$$

$$u_x = \frac{u_x^*}{m\omega_0^2 q_0} \qquad u_y = \frac{u_y^*}{m\omega_0^2 q_0} \tag{5}$$

$$\omega_x = \sqrt{\frac{k_{xx}}{m\omega_0^2}} \qquad \omega_y = \sqrt{\frac{k_{yy}}{m\omega_0^2}} \qquad \omega_{xy} = \frac{k_{xy}}{m\omega_0^2} \tag{6}$$

where each axis' natural frequency is ω_0 and the reference length is q_0.

The following are the dynamic equations for the MEMS gyroscope.

$$\ddot{q} = -(D + 2\Omega)\dot{q} - K_b q - \beta q^3 + u + E \tag{7}$$

An external disturbance, *E*, might be modeled as:

$$\ddot{q} = -Y\dot{q} - Pq - \beta q^3 + u + E \tag{8}$$

where Y and P determine certain parameter variation uncertainties, $P = K_b$ and $Y = (D + 2\Omega)$. Therefore, Eq. (8) might be expressed as:

$$\ddot{q} = -(Y + \Delta Y)\dot{q} - (P + \Delta P)q - \beta q^3 + u + E \tag{9}$$

where

$$q = \begin{bmatrix} x \\ y \end{bmatrix}, u = \begin{bmatrix} u_x \\ u_y \end{bmatrix}, \Omega = \begin{bmatrix} 0 & -\Omega_z \\ \Omega_z & 0 \end{bmatrix}, D = \begin{bmatrix} d_{xx} & d_{xy} \\ d_{xy} & d_{yy} \end{bmatrix}, K_b = \begin{bmatrix} \omega_x^2 & \omega_{xy} \\ \omega_{xy} & \omega_y^2 \end{bmatrix}$$

There are several ways to show Eq. (9):

$$\ddot{q} = -Y\dot{q} - Pq - \beta q^3 + u(t) + D(t) \tag{10}$$

D(t) describes as:

$$D(t) = -\Delta Y\dot{q} - \Delta Pq + E \tag{11}$$

The expression for Eq. (10) in the x and y directions is

$$\begin{bmatrix} \ddot{x} \\ \ddot{y} \end{bmatrix} = -\left(\begin{bmatrix} d_{xx} & d_{xy} \\ d_{xy} & d_{yy} \end{bmatrix} + \begin{bmatrix} 0 & -2\Omega_z \\ 2\Omega_z & 0 \end{bmatrix}\right)\begin{bmatrix} \dot{x} \\ \dot{y} \end{bmatrix} - \begin{bmatrix} \omega_x^2 & \omega_{xy} \\ \omega_{xy} & \omega_y^2 \end{bmatrix}\begin{bmatrix} x \\ y \end{bmatrix} - \tag{12}$$

$$\begin{bmatrix} \beta & 0 \\ 0 & \beta \end{bmatrix}\begin{bmatrix} x^3 \\ y^3 \end{bmatrix} + \begin{bmatrix} 1 & 0 \\ 0 & 1 \end{bmatrix}\begin{bmatrix} u_x \\ u_y \end{bmatrix} + \quad + \begin{bmatrix} D(t)_x \\ D(t)_y \end{bmatrix}$$

Eq. (12) will be transformed into first-order dynamic equations by selecting the following parameters:

$$\begin{cases} x = z_1 \\ \dot{x} = z_2 \\ y = z_3 \\ \dot{y} = z_4 \end{cases}$$

Then, there is

$$\begin{cases} \dot{z}_1 = z_2 \\ \dot{z}_2 = -\omega_x^2 z_1 - \beta z_1^3 - d_{xx} z_2 - \omega_{xy} z_3 + \left(2\Omega_z - d_{xy}\right) z_4 + u_{z_1} + D_{z_1} \\ \dot{z}_3 = z_4 \\ \dot{z}_4 = -\omega_{xy} z_1 - \left(d_{xy} + 2\Omega_z\right) z_2 - \omega_y^2 z_3 - \beta z_3^3 - d_{yy} z_4 + u_{z_3} + D_{z_3} \end{cases} \tag{13}$$

Equation (13) shows

$$\dot{z} = A(z) + Bu \tag{14}$$

Eq. (14) can be written in its classical form as follows:

$$\frac{d}{dt}z(t) = f(z) \tag{15}$$

3- Koopman theory

According to the Koopman operator theory, the crucial step to correctly a non-linear dynamical system is to transform the non-linear system's original form into an infinite dimensional state space so that the resulting system is linear [15].

The dynamic in discrete time defines as [31]:

$$z_{k+1} = F(z_k) \tag{16}$$

where F is characterized by

$$F\big(z(t_0)\big) = z(t_0) + \int_{t_0}^{t_0+t} f\big(z(\tau)\big)d\tau \tag{17}$$

When a finite-dimensional non-linear system's dynamics are transferred to an infinite-dimensional function space using the Koopman operator theoretic method, the original system's dynamics become linear. *g* is a real-valued scalar measurement function and an observable part of an infinite-dimensional Hilbert space. The Koopman operator generates based on this observable as

$$Kg = g \circ F \tag{18}$$

Smooth dynamics can be implemented using a continuous system.

$$\frac{d}{dt}g(z) = Kg(z) = \nabla g(z).f(z) \tag{19}$$

where the Koopman operator is K. The infinite dimensions of the Koopman operator are significant but problematic for operation and representation. Instead of describing the development of all measurement functions in a Hilbert space, applied Koopman analysis approximates the evolution on a subspace covered by a small number of measurement functions. One can get a representation of the Koopman operator in a finite-dimensional matrix by limiting the operator to an invariant subspace. A Koopman invariant subspace is covered by any combination of the eigenfunctions of

the Koopman operator [31]. When eigenvalue λ is satisfied by eigenfunction $\varphi(z)$ of the Koopman model.

$$\lambda\varphi(z) = \varphi\big(F(z)\big) \tag{20}$$

In continuous time, a Koopman eigenfunction $\varphi(z)$ is satisfied.

$$\frac{d}{dt}\varphi(z) = \lambda\varphi(z) \tag{21}$$

A finite-dimensional approximation is required from the application side to approximate the Koopman operator. DMD method is one of the approaches that can estimate the Koopman operator [31].

4- DMD method

A numerical DMD is utilized to approximate the Koopman operator.

$$Z' \approx AZ \tag{22}$$

where $Z'$is time-shifted of matrix Z as:

$Z = [z_1 \quad z_2 \quad \dots\dots]$

The A can be found according to Eq. (22) as:

$$A = Z'Z^{+} \tag{23}$$

where + represents the Moore-Penrose pseudoinverse. We may use Singular Value Decomposition (SVD) on the snapshots to determine the dominating properties of the pseudoinverse of Z because a typical calculation involving A would need a significant amount of computation due to its size [32].

$$Z \approx U\Sigma V^{*} \tag{24}$$

where $U \in R^{n\times r}$, $\Sigma \in R^{r\times r}$, $V \in R^{n\times r}$, and * demonstrate the conjugate transpose. SVD's reduced rank for approximating Z is r. The eigenvectors can be defined as:

$$\Phi = Z'V\Sigma^{-1}\mathrm{W} \tag{25}$$

where W is the eigenvectors of full-rank system dynamic systems.

$$\Phi = Z'V\Sigma^{-1}\mathrm{W} \tag{26}$$

Let λ be eigenfunction, and then we will have:

$$KW = \lambda W \tag{27}$$

where *K* is the Koopman operator.

The linearized dynamic model can be demonstrated as:

$$\frac{d}{dt}y = Ky + Bu \tag{28}$$

5- FOPID control

PID controller is a suitable control method used in many industrial applications [33-35]. It constantly evaluates the error using its parameters K_p, K_i, and K_d and delivers the correct value. The PID controller can be defined as:

$$u_{PID} = K_p e(t) + K_i \int_0^t e(\tau)d\tau + K_d \frac{de(t)}{dt} \tag{29}$$

where $e(t) = y - y_d$, which y_d is the desired trajectory.

The main problem of the PID controller is that it's not robust against external disturbances. Also, the stability of the PID controller is another issue that should be considered during the controller design.

A fractional control method can be used to improve the controller's performance. In addition, it can improve the stability and robustness of a typical PID controller. The FOPID controller can be defined as:

$$u_{FOPID} = K_p e(t) + K_i D^{-\mu} e(t) + K_d D^{\mu} e(t) \tag{30}$$

where *D* is a fractional operator defined as $D = \frac{d}{dt}$ and μ is fractional order. The fractional type that we use in this research is Grunwald-Letnikov [36]. The Grunwald-Letnikov fractional derivative of the function *e(t)* with respect to *t* is given

$$D_t^{\mu} e(t) = lim_{h \to 0} h^{-\mu} \sum_{k=0}^{n} (-1)^k \binom{\mu}{k} f(e(t) - kh) \tag{31}$$

where

$$\binom{\mu}{k} = \frac{\mu(\mu-1)(\mu-2)\dots(\mu-k+1)}{k!} = \frac{\Gamma(\mu+1)}{k!\,\Gamma(\mu-k+1)}$$

A detailed explanation is given in [36]. The control structure shows in Fig. 2.

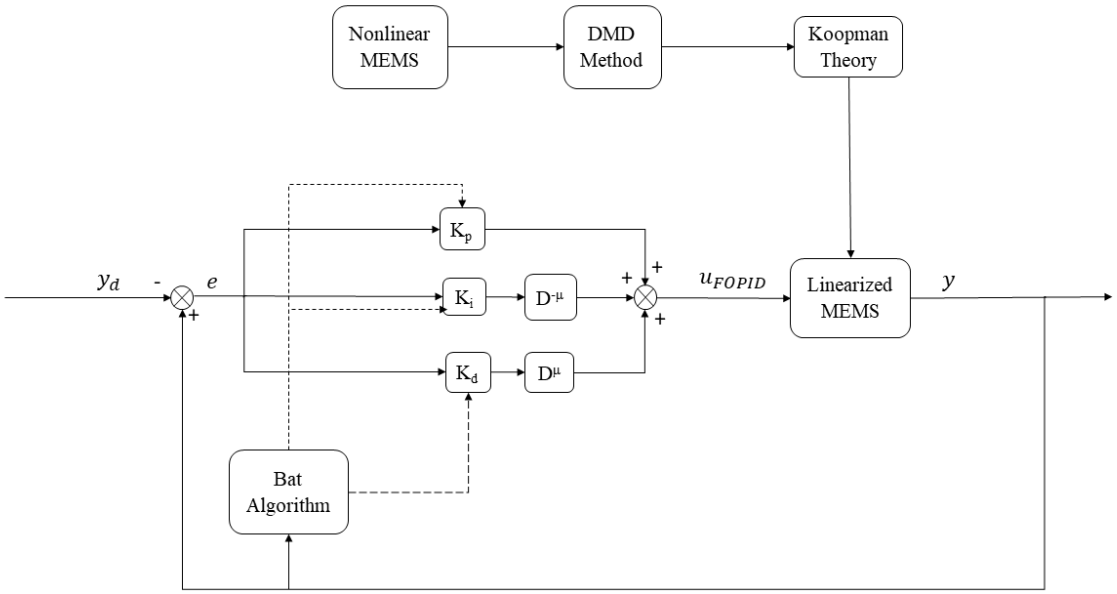

Fig. 2. The proposed control structure.

One of the main parts of FOPID controller design is how to tune the controller's parameters. The metaheuristic algorithms are rich sources to adjust the FOPID controller parameters.

6- Bat algorithm to tune the proposed controller parameters

The optimization technique known as the bio-inspired bat algorithm was influenced by how bats use echolocation to find food. It was introduced in [37, 38] and used to resolve several optimization issues. The echolocation strategy of bats is used in the algorithm. These bats create an extremely loud sound pulse; then, they listen for the echo returned from the nearby objects. Depending on

the species, their signal bandwidth ranges change through harmonics. The i^{th} bat moves randomly at location x_i with velocity v_i and a set frequency f_{min}. To discover food, the bat changes its wavelength and volume. To improve the echolocation capabilities, an objective function needs to be optimized. Developing an optimization algorithm from how a bat searches for the best answer is possible. The algorithms for bat-inspired echolocation can be created by enhancing certain of the microbats' echolocation characteristics. The bat echolocation features to address an optimization issue brought about by the following hypotheses [39].

1- An echolocation is a tool used by all bats to detect distance.

2- To locate prey, bats fly at random speeds of v_i at positions x_i with a fixed frequency and wavelength of f_{min} and a variable wavelength and frequency of A_0.

3- Depending on how close the prey is, they can control their wavelength/frequency and pulse emission rate, $r_i \in$ [0-1].

4- Their loudness decreases from high A_0 to low A_{min} levels as they get closer to the prey.

In actual implementations, frequency occurs between [f_{min}, f_{max}] and is chosen to be similar to the size of the domain of interest. For a virtual bat to solve an optimization issue, rules must be developed to specify their locations and velocities in the d-dimensional search space. The following definitions apply to the new location x_i^+ and velocity v_i^+ at time step t [40].

$$f_i = f_{min} + (f_{max} - f_{min})\xi \tag{32}$$

$$v_i^t = v_i^{t-1} + (x_i^{t-1} - x^*)f_i \tag{33}$$

$$x_i^t = x_i^{t-1} + v_i^t \tag{34}$$

The current best solution across all N bats is represented by x^*, where $\xi \in$ [0-1] is the random vector generated randomly from a uniform distribution. When a new solution is needed for local search, it is determined using the most recent bat loudness A_i and the most variance that can be tolerated max(var) at a time stop, as shown below.

$$x_{new} = x_{old} + \varepsilon A_i \max(var) \tag{35}$$

The volume drops, and the pulse emission rate rises as a bat locates its prey. The bat is heading towards the target, as shown by

$$A_i^{t+1} = \alpha A_i^t, \quad r_i^{t+1} = r_r^{\circ}[1 - e^{-\gamma t}] \tag{36}$$

Where α and γ are constant. Initial boundness is $A_i \in [0.1\text{-}0.9]$, initial emission rate is $r_0 \in [0\text{-}1]$, and $\alpha = \gamma = 0.9$. The bat algorithm is used for tuning the [K_p, K_i, K_d] parameters of the proposed controller for a MEMS gyroscope. This problem's objective function is described as follows [16]:

$$J = \int_0^{\infty} (w_1 |e(t)| + w_2 u^2(t)) dt + w_3 t_u \tag{37}$$

7- Simulation results

A MEMS gyroscope is controlled using the proposed Koopman-BAFOPID controller. Additionally, several comparative methods are used to show how effective the proposed Bat algorithm is in adjusting the Koopman-FOPID parameters. The non-linear dynamic equations of a MEMS gyroscope are generated in this research. All simulation steps are simulated using Matlab software. Fig. 3 shows the flow chart of the bat algorithm steps in tuning the Koopman-FOPID controller. The parameters of the proposed controller in this study are as follows: total population = 5; iteration = 20; loudness = 0.5; wavelength = 0.5; frequency f_{min} = 10, f_{max} = 20.

The objective function variables are set to w_1=0.99, w_2=0.01, and w_3=2. The tuned parameters of bat algorithm are K_p=diag{17.9901}, K_i={22.3411}, and K_d={27.2585}.

Fig. 4 shows the trajectory tracking of x and y direction under PID, FOPID, Koopman-FOPID, and Koopman-BAFOPID controllers. It demonstrates that the proposed Koopman-BAFOPID controller has a high tracking performance compared to the three other controllers. Fig. 5 shows the position tracking error of x and y directions under PID, FOPID, Koopman-FOPID, and Koopman-BAFOPID controllers. It illustrates that the proposed Koopman-BAFOPID controller has low tracking error in comparison with the PID, FOPID, Koopman-FOPID, and Koopman-BAFOPID controllers. Fig. 6 show the velocity of x and y direction under PID, FOPID, Koopman-FOPID, and Koopman-BAFOPID controllers. First, a conventional PID controller is applied to a non-linear MEMS gyroscope to control the x and y direction. The main problem with that controller is that it's not stable. Then, a FOPID controller is used to remove conventional PID controllers' stability problem. Fig. 7 shows the control inputs under PID, FOPID, Koopman-FOPID, and Koopman-BAFOPID controllers. It demonstrates that the PID controller is unstable by increasing the control efforts when time increases, but the FOPID controller fixed this problem.

Therefore, using the FOPID controller provides better stability, along with using Koopman theory on a non-linear MEMS gyroscope.

8. Conclusion

This paper proposed a new Koopman-BAFOPID control of a non-linear MEMS gyroscope. The PID controller stability improved by presenting the FOPID controller. The Koopman theory is used to derive a linear dynamic model of the MEMS gyroscope. The DMD method was used to estimate the Koopman operators numerically. Then, the selected FOPID controller was then applied to a linearized MEMS gyroscope dynamic model to suitably controlling the x and y direction. A bat algorithm was implemented on the Koopman-FOPID controller to tune the proposed controller parameters. The simulation results verified that the proposed Koopman-BAFOPID controller has better performance than PID, FOPID, and Koopman-FOPID controllers in terms of high tracking performance, low tracking error, low control efforts, and increased stability.

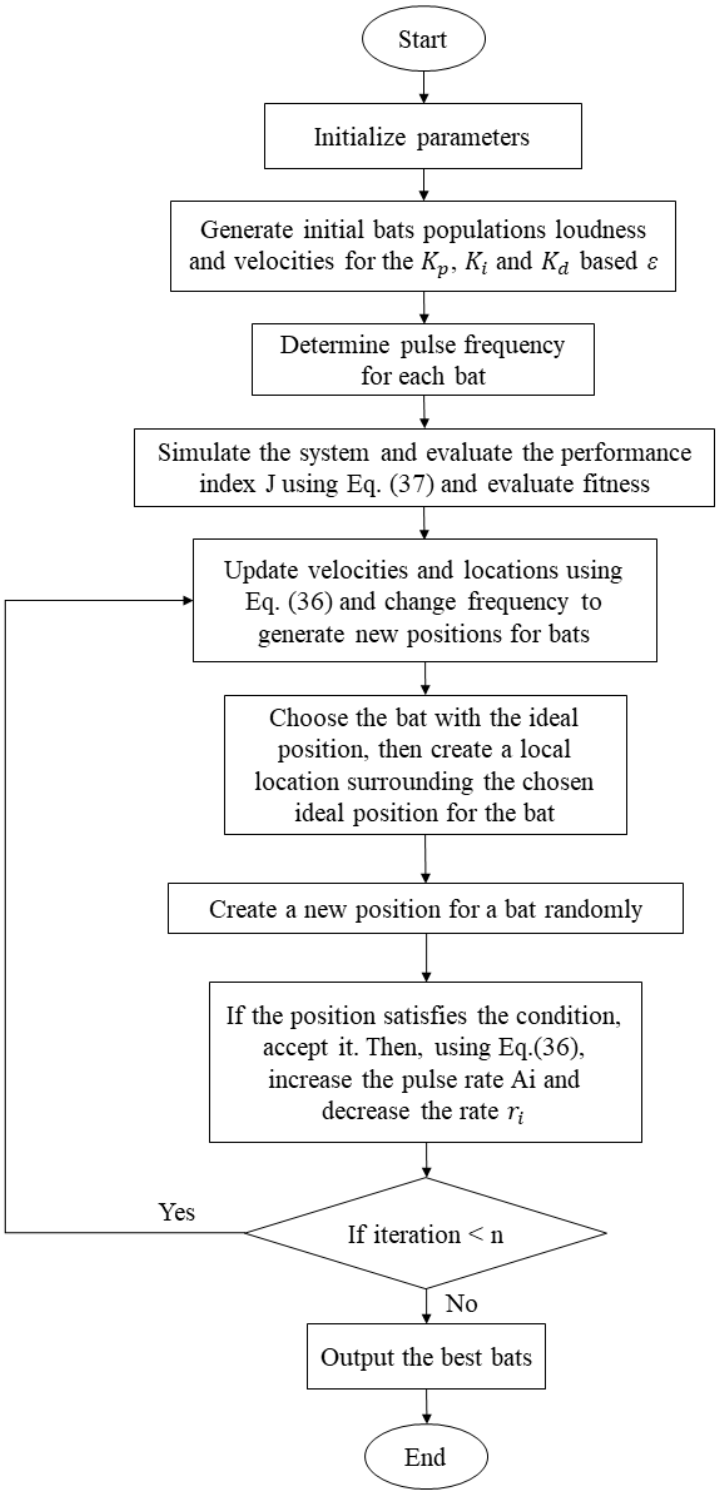
Start
Initialize parameters
Generate initial bats populations loudness and velocities for the K_p, K_i and K_d based ε
Determine pulse frequency for each bat
Simulate the system and evaluate the performance index J using Eq. (37) and evaluate fitness
Update velocities and locations using Eq. (36) and change frequency to generate new positions for bats
Choose the bat with the ideal position, then create a local location surrounding the chosen ideal position for the bat
Create a new position for a bat randomly
If the position satisfies the condition, accept it. Then, using Eq.(36), increase the pulse rate Ai and decrease the rate r_i
If iteration < n
Yes
No
Output the best bats
End

Fig. 3. Flow chart for a bat algorithm for tuning Koopman-FOPID parameters.

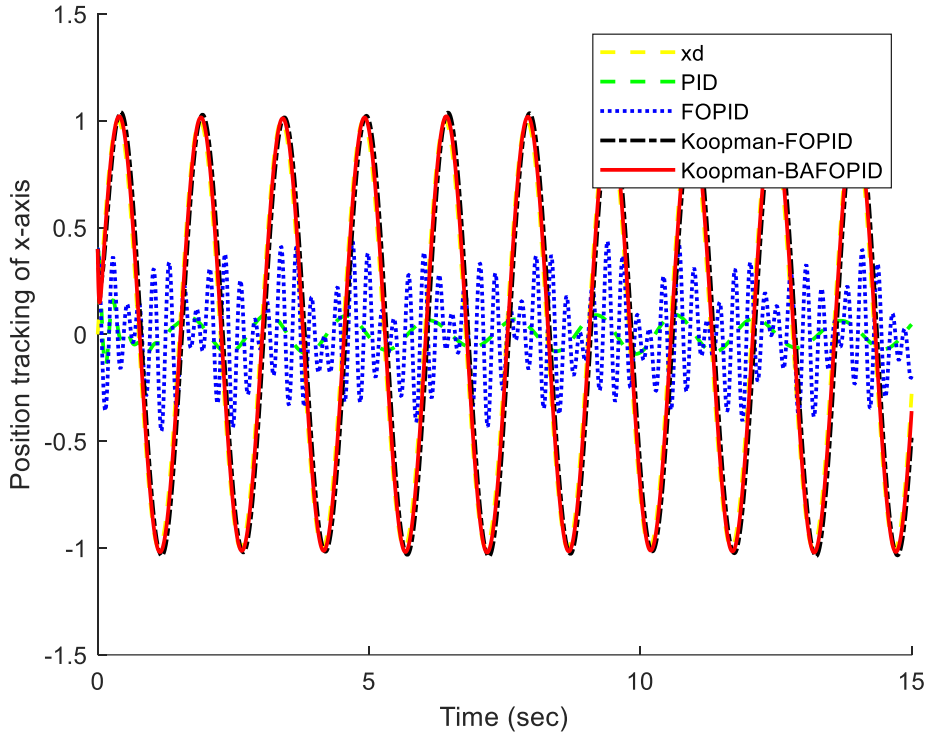

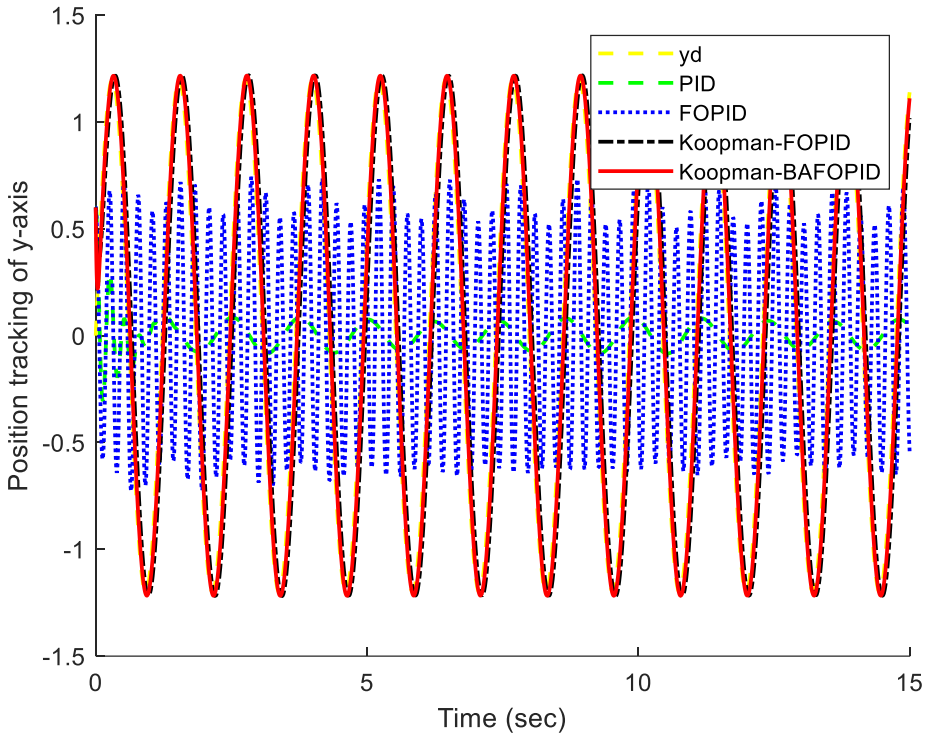

Fig. 4. Position tracking of x and y under the proposed controllers.

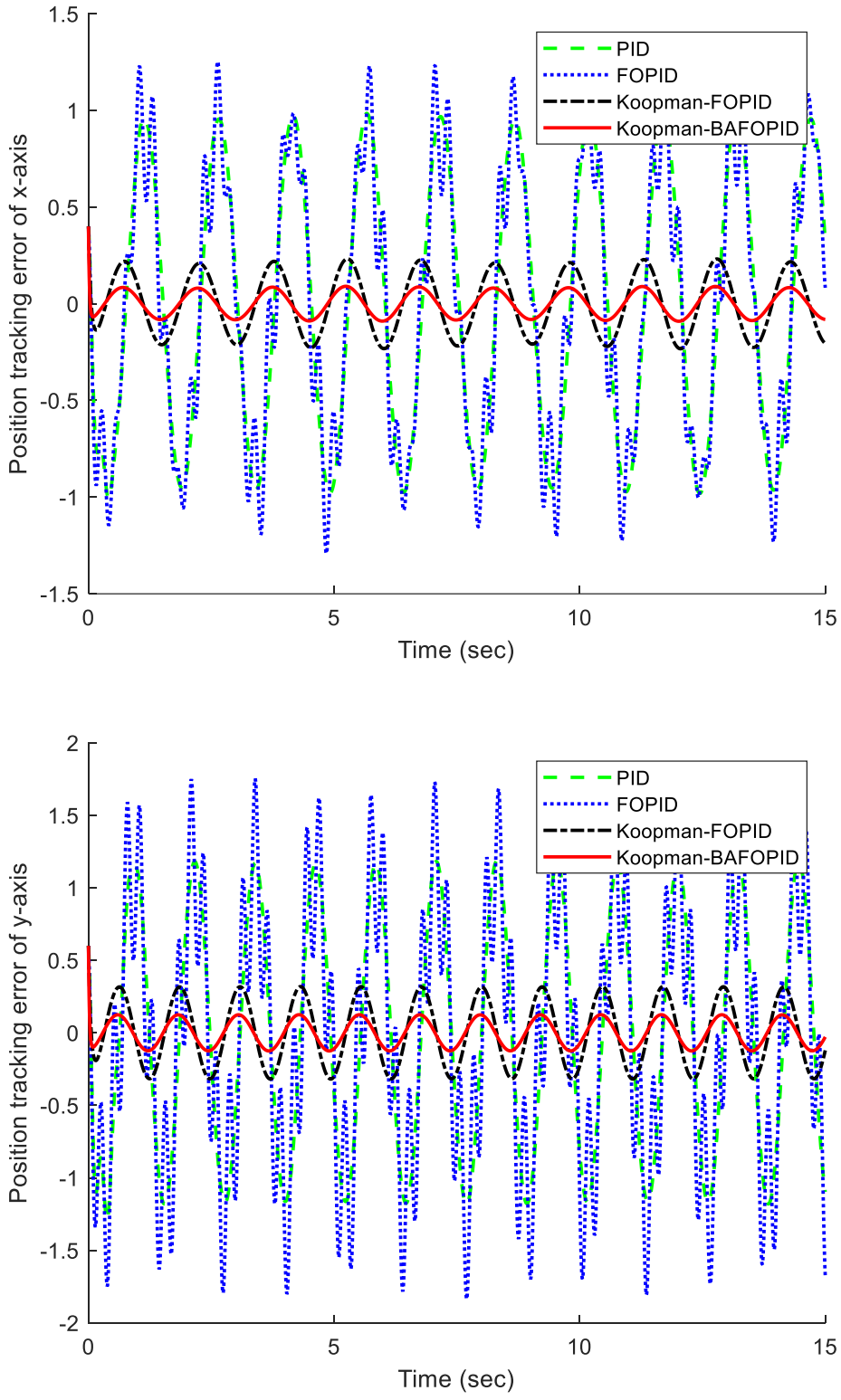

Fig. 5. Position tracking error of x and y directions under the proposed controllers.

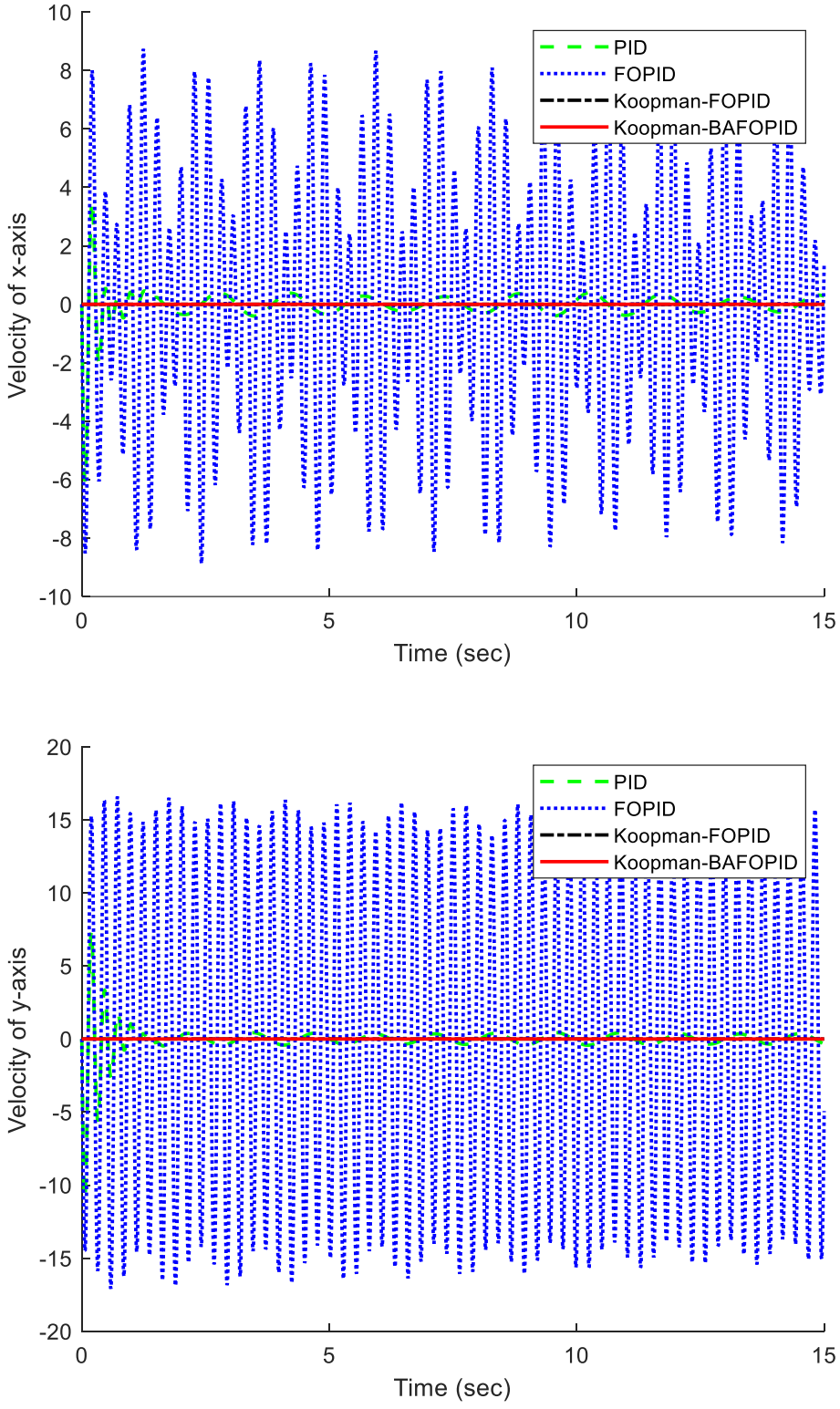

Fig. 6. Velocity of x and y directions under the proposed controllers.

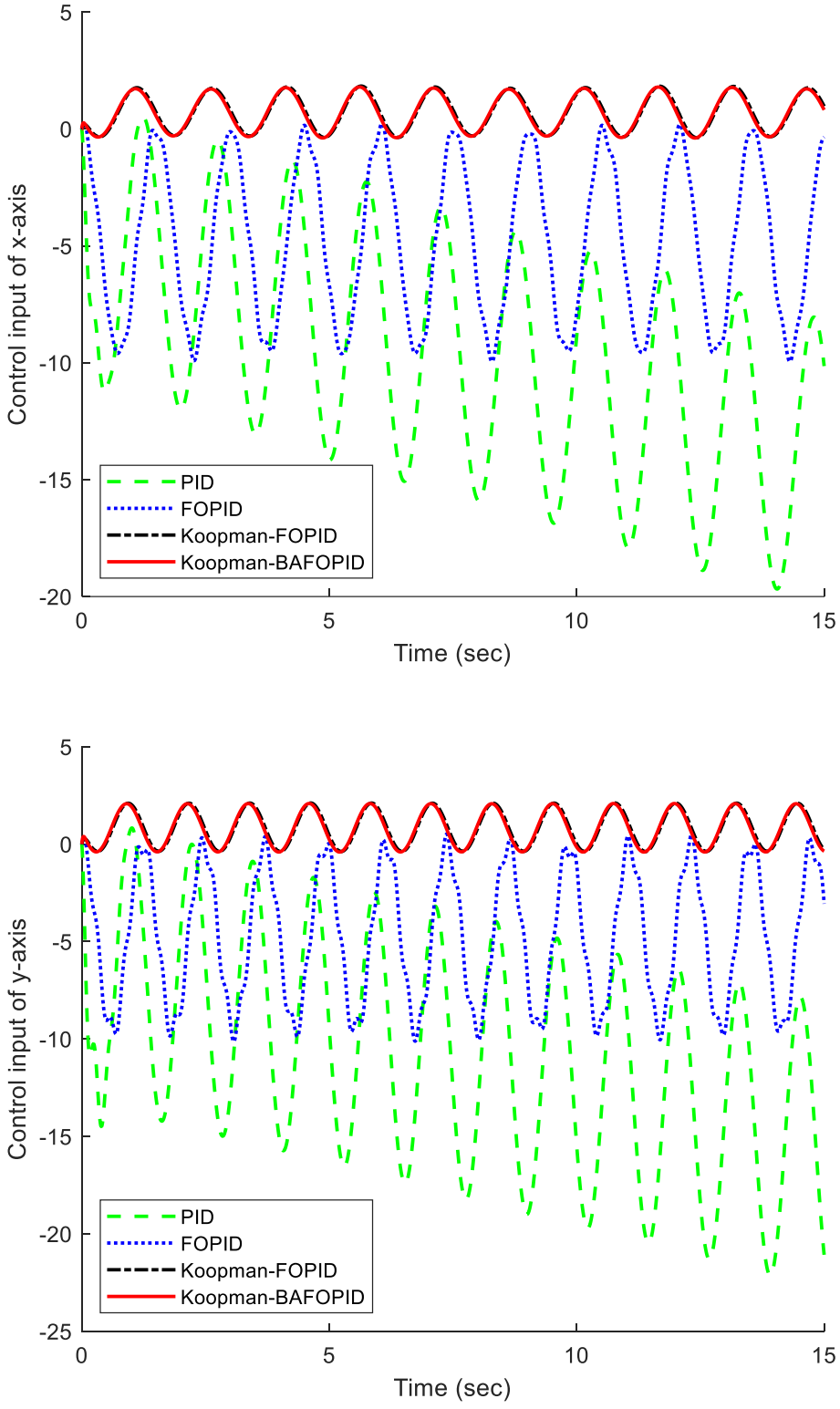

Fig. 7. Velocity of x and y directions under the proposed controllers.

References

[1] Solouk, M. R., Shojaeefard, M. H., & Dahmardeh, M. (2019). Parametric topology optimization of a MEMS gyroscope for automotive applications. *Mechanical Systems and Signal Processing*, 128, 389-404.

[2] Classen, J., Frey, J., Kuhlmann, B., Ernst, P., & Bosch, R. (2007, August). MEMS gyroscopes for automotive applications. In *Advanced Microsystems for Automotive Applications* (pp. 291-306). Berlin, Germany: Springer.

[3] Gao, S., Liu, L., Wang, H., & Wang, A. (2022). Data-driven model-free resilient speed control of an Autonomous Surface Vehicle in the presence of actuator anomalies. *ISA Transactions*.

[4] Xian, B., Gu, X., & Pan, X. (2022). Data driven adaptive robust attitude control for a small size unmanned helicopter. *Mechanical Systems and Signal Processing*, 177, 109205.

[5] Liu, H., Cheng, Q., Xiao, J., & Hao, L. (2021). Data-driven adaptive integral terminal sliding mode control for uncertain SMA actuators with input saturation and prescribed performance. *ISA transactions*.

[6] Sun, C., Dominguez-Caballero, J., Ward, R., Ayvar-Soberanis, S., & Curtis, D. (2022). Machining cycle time prediction: Data-driven modeling of machine tool feed rate behavior with neural networks. *Robotics and Computer-Integrated Manufacturing*, 75, 102293.

[7] Chen, W. H., & You, F. (2021). Semiclosed greenhouse climate control under uncertainty via machine learning and data-driven robust model predictive control. *IEEE Transactions on Control Systems Technology*, 30(3), 1186-1197.

[8] Goswami, D., & Paley, D. A. (2021). Bilinearization, reachability, and optimal control of control-affine non-linear systems: A Koopman spectral approach. *IEEE Transactions on Automatic Control*.

[9] Bruder, D., Fu, X., Gillespie, R. B., Remy, C. D., & Vasudevan, R. (2020). Data-driven control of soft robots using Koopman operator theory. *IEEE Transactions on Robotics*, 37(3), 948-961.

[10] Zanini, F., & Chiuso, A. (2021). Estimating Koopman operators for non-linear dynamical systems: a nonparametric approach. IFAC-PapersOnLine, 54(7), 691-696.

[11] Jiang, L., & Liu, N. (2022). Correcting noisy dynamic mode decomposition with Kalman filters. *Journal of Computational Physics*, 461, 111175.

[12] Ling, E., Zheng, L., Ratliff, L. J., & Coogan, S. (2020). Koopman operator applications in signalized traffic systems. *IEEE Transactions on Intelligent Transportation Systems*.

[13] Wilches-Bernal, F., Reno, M. J., & Hernandez-Alvidrez, J. (2021). A Dynamic Mode Decomposition Scheme to Analyze Power Quality Events. *IEEE Access*, *9*, 70775-70788.

[14] Mamakoukas, G., Castano, M., Tan, X., & Murphey, T. (2019, June). Local Koopman operators for data-driven control of robotic systems. In Robotics: science and systems.

[15] Ping, Z., Yin, Z., Li, X., Liu, Y., & Yang, T. (2021). Deep Koopman model predictive control for enhancing transient stability in power grids. *International Journal of Robust and Nonlinear Control*, 31(6), 1964-1978.

[16] Rahmani, M., Ghanbari, A., & Ettefagh, M. M. (2016). Robust adaptive control of a bio-inspired robot manipulator using bat algorithm. *Expert Systems with Applications*, 56, 164-176.

[17] Rahmani, M., Komijani, H., Ghanbari, A., & Ettefagh, M. M. (2018). Optimal novel super-twisting PID sliding mode control of a MEMS gyroscope based on multi-objective bat algorithm. *Microsystem Technologies*, 24(6), 2835-2846.

[18] Fei, J., & Chu, Y. (2016, August). Dynamic global PID sliding mode control for MEMS gyroscope using an adaptive neural controller. In 2016 Joint 8th International Conference on Soft Computing and Intelligent Systems (SCIS) and the 17th International Symposium on Advanced Intelligent Systems (ISIS) (pp. 16-21). IEEE.

[19] Marino, R., Scalzi, S., & Netto, M. (2011). Nested PID steering control for lane keeping in autonomous vehicles. *Control Engineering Practice*, 19(12), 1459-1467.

[20] Yoon, J., & Doh, J. (2022). Optimal PID control for hovering stabilization of quadcopter using long short-term memory. *Advanced Engineering Informatics*, 53, 101679.

[21] Liu, L., Zhang, L., Pan, G., & Zhang, S. (2022). Robust yaw control of autonomous underwater vehicle based on fractional-order PID controller. *Ocean Engineering*, 257, 111493.

[22] Erol, H. (2021). Stability analysis of pitch angle control of large wind turbines with fractional order PID controller. *Sustainable Energy, Grids and Networks*, 26, 100430.

[23] Yang, X. S. (2010). A new metaheuristic bat-inspired algorithm. In *Nature inspired cooperative strategies for optimization* (NICSO 2010) (pp. 65-74). Springer, Berlin, Heidelberg.

[24] Lakshmanaprabu, S. K., Elhoseny, M., & Shankar, K. (2019). Optimal tuning of decentralized fractional order PID controllers for TITO process using the equivalent transfer function. *Cognitive Systems Research*, 58, 292-303.

[25] Chaib, L., Choucha, A., & Arif, S. (2017). Optimal design and tuning of novel fractional order PID power system stabilizer using a new metaheuristic Bat algorithm. *Ain Shams Engineering Journal*, 8(2), 113-125.

[26] Fang, Y., Fu, W., Ding, H., & Fei, J. (2022). Modeling and neural sliding mode control of mems triaxial gyroscope. *Advances in Mechanical Engineering*, 14(3), 16878132221085876.

[27] Lu, C., & Fei, J. (2016, June). Adaptive sliding mode control of MEMS gyroscope with prescribed performance. In the 2016 14th International Workshop on Variable Structure Systems (VSS) (pp. 65-70). IEEE.

[28] Guo, Y., Xu, B., & Zhang, R. (2020). Terminal sliding mode control of mems gyroscopes with finite-time learning. *IEEE Transactions on Neural Networks and Learning Systems*, 32(10), 4490-4498.

[29] Rahmani, M., Rahman, M. H., & Nosonovsky, M. (2020). A new hybrid robust control of MEMS gyroscope. *Microsystem Technologies*, 26(3), 853-860.

[30] Yan, W., Hou, S., Fang, Y., & Fei, J. (2017). Robust adaptive nonsingular terminal sliding mode control of MEMS gyroscope using fuzzy-neural-network compensator. *International Journal of Machine Learning and Cybernetics*, 8(4), 1287-1299.

[31] Kaiser, E., Kutz, J. N., & Brunton, S. L. (2021). Data-driven discovery of Koopman eigenfunctions for control. *Machine Learning: Science and Technology*, 2(3), 035023.

[32] Snyder, G., & Song, Z. (2021). Koopman Operator Theory for Nonlinear Dynamic Modeling using Dynamic Mode Decomposition. arXiv preprint arXiv:2110.08442.

[33] Malarvili, S., & Mageshwari, S. (2022). Nonlinear PID (N-PID) Controller for SSSP Grid Connected Inverter Control of Photovoltaic Systems. *Electric Power Systems Research*, 211, 108175.

[34] Guo, T. Y., Lu, L. S., Lin, S. Y., & Hwang, C. (2022). Design of maximum-stability PID controllers for LTI systems based on a stabilizing-set construction method. *Journal of the Taiwan Institute of Chemical Engineers*, 135, 104366.

[35] Yan, L., Webber, J. L., Mehbodniya, A., Moorthy, B., Sivamani, S., Nazir, S., & Shabaz, M. (2022). Distributed optimization of heterogeneous UAV cluster PID controller based on machine learning. *Computers and Electrical Engineering*, 101, 108059.

[36] Abdelouahab, M. S., & Hamri, N. E. (2016). The Grünwald–Letnikov fractional-order derivative with fixed memory length. *Mediterranean Journal of Mathematics*, 13(2), 557-572.

[37] Yang, X. S. (2010). A new metaheuristic bat-inspired algorithm. In Nature inspired cooperative strategies for optimization (NICSO 2010) (pp. 65-74). Springer, Berlin, Heidelberg.

[38] Yang, X. S. (2012). Bat algorithm for multi-objective optimization. arXiv preprint arXiv:1203.6571.

[39] Sathya, M. R., & Ansari, M. M. T. (2015). Load frequency control using bat-inspired algorithm-based dual mode gain scheduling of PI controllers for interconnected power system. *International Journal of Electrical Power & Energy Systems*, 64, 365-374.

[40] Mitić, M., & Miljković, Z. (2015). Bio-inspired approach to learning robot motion trajectories and visual control commands. *Expert Systems with Applications*, 42(5), 2624-2637.